https://doi.org/10.1016/j.scs.2021.103583
Dai, T., Liu, S., Liu, J., Jiang, N., Liu, W., and Chen, Q. 2022. "Evaluation of fast fluid dynamics with different turbulence models for predicting outdoor airflow and pollutant dispersion," Sustainable Cities and Society, 77: 103583.

Evaluation of fast fluid dynamics with different turbulence models for predicting outdoor airflow and pollutant dispersion

Ting Dai [a], Sumei Liu [a,*], Junjie Liu [a], Nan Jiang [b], Wei Liu [c], Qingyan Chen [d]

[a] *Tianjin Key Laboratory of Indoor Air Environmental Quality Control, School of Environmental Science and Engineering, Tianjin University, Tianjin 300072, China*

[b] *School of Mechanical Engineering, Tianjin University, Tianjin 300072, China*

[c] *Division of Sustainable Buildings, Department of Civil and Architectural Engineering, KTH Royal Institute of Technology, Brinellv¨agen 23, Stockholm, 10044, Sweden*

[d] *Department of Building Environment and Energy Engineering, The Hong Kong Polytechnic University, Kowloon, 999077, Hong Kong SAR, China*

***Corresponding author. *E-mail addresses:* daiting@tju.edu.cn (T. Dai), smliu@tju.edu.cn (S. Liu), jjliu@tju.edu.cn (J. Liu), nanj@tju.edu.cn (N. Jiang), weiliu2@kth.se (W. Liu), qingyan.chen@polyu.edu.hk (Q. Chen).**

ABSTRACT

Fast fluid dynamics (FFD) could provide informative and efficient airflow and concentration simulation. The commonly used turbulence model in FFD was Re-Normalization Group (RNG) k-ε turbulence model which solved two transport equations to obtain eddy viscosity. To reduce this part of time and further improve computing speed, this investigation implemented no turbulence model, Smagorinsky model and dynamic Smagorinsky model which calculated eddy viscosity without solving equation in FFD in an open-source program, OpenFOAM. By simulating several outdoor cases of varying complexity and comparing with experiment and CFD, this study assessed the accuracy and computing efficiency of FFD with four turbulence models. Compared with CFD, FFD greatly improved the computing speed without reducing accuracy. The simulation of FFD without turbulence model was fast but inaccurate. FFD with Smagorinsky model increased the computing speed while ensuring the same accuracy as RNG k-ε turbulence model. FFD with dynamic Smagorinsky model provided accurate results with high efficiency. Computation errors arose mainly from inaccurate prediction of turbulence dispersion. The computing cost was associated with the number of transport equations and calculation method of model coefficient. This investigation recommended the use of FFD with dynamic Smagorinsky model for outdoor airflow and pollutant dispersion studies.

Keywords: fast fluid dynamics, turbulence model, outdoor airflow, pollutant dispersion, computational efficiency

1. Introduction

The process of industrialization has brought many challenges, such as the increased pollutant discharged into the outdoor environment, resulting in air quality degradation (Cole, Elliott, & Shimamoto, 2005; Li, Li, & Zhang, 2018). Some pollutants were not discharged at high altitude where they would be effectively diluted; instead, they spread around buildings. Due to the

complex flow around buildings, released pollutants not only re-entered the building where they were released from, but also affected neighboring buildings (Hajra, Stathopoulos, & Bahloul, 2010; Petersen, Cochran, & Carter, 2002). This caused secondary pollution and posed a threat to the health of building occupants. To avoid this secondary pollution, it was necessary to study the airflow and pollutant diffusion in the outdoor area.

Research methods for airflow and pollutant diffusion in outdoor environment included wind tunnel experiment, analytical methods and numerical simulation (Stathopoulos, Hajra, & Bahloul, 2008). Wind tunnel experiment was found to be more convenient than field test, and the experimental conditions could be effectively controlled and adjusted (Lin, Ooka, Kikumoto, & Sato, 2020; Palida, Yu, & Wu, 2009). However, the wind tunnel experiment was expensive and time-consuming. In addition, it generally only provided a limited amount of data at discrete measuring locations (Gousseau, Blocken, Stathopoulos, & van Heijst, 2011). Meanwhile, analytical models, such as the Gaussian dispersion model, used mathematical equations which described key physical processes to estimate pollutant concentration (Ebrahimi, & Jahangirian, 2013; Holmes, & Morawska, 2006; Mangia, Degrazia, & Rizza, 2000; Overcamp, 1976; Lotrecchiano, Sofia, Giuliano, Barletta, & Poletto, 2020). The main advantages of the Gaussian model were high computation speed and low data input requirements. However, due to the various simplifications in the model, it was impossible to accurately describe the turbulence of the airflow and the pollutant dispersion in complex outdoor environment (Stathopoulos, Hajra, & Bahloul, 2008; Yu, & The, 2017).

With the development of computer resources, computational fluid dynamics (CFD) method has been increasingly used to study the airflow and pollutant dispersion around buildings, ranging from a single building to an urban block (Blocken, Stathopoulos, Carmeliet, & Hensen, 2009; He, Liu, Zhang, & Zheng, 2021; Jandaghian, 2018; Tominaga, & Mochida, 2016; Liu, Pan, Zhang, Cheng, & Long, 2017; Mei, Luo, Zhao, & Wang, 2019; Qin, Hong, Huang, Cui, & Zhang, 2020; Tominaga, Mochida, Murakami, & Sawaki, 2008; Tominaga et al., 2008; Tominaga, & Stathopoulos, 2010; Zhang et al., 2021). By solving the Navier-Stokes equations, CFD could provide data for the entire flow field. Previous studies have proved the effectiveness of CFD in simulating outdoor environments. However, the main limitation of CFD in simulating outdoor airflow was the high computing cost. For example, it took more than 100 hours to simulate the airflow in a small urban region with around one million cells (Tseng, Meneveau, & Parlange, 2006).

Computation efficiency was of great importance in engineering applications. Fast fluid dynamics (FFD) could provide rapid and informative simulation of outdoor airflow and pollution dispersion. Previous investigations found that FFD was 50 times faster than CFD (Zuo, & Chen, 2009). Stam (Stam, 1999) firstly proposed FFD for fluid flow visualization in computer games. Fedkiw (Fedkiw, Stam, & Jensen, 2001) applied FFD to simulate smoke motion in practical application. The original FFD developed by Stam assumed the flow to be laminar, and the assumption was adopted in simulating indoor airflow, turbulent flow with forced convection, and natural ventilation when it was first introduced to buildings (Zuo, & Chen, 2010; Zuo, Hu, & Chen, 2010; Jin, Liu, & Chen, 2014). Later, turbulence models were added to FFD for greater accuracy. For example, the RNG k-ε turbulence model was implemented in FFD to simulate the airflow in a room and it had similar computational accuracy as that of CFD (Liu, You, Zhang, & Chen, 2017). However, this turbulence model needed to solve multiple partial differential equations, and it required more computing time. Some researches applied the zero-equation model which was proposed by Chen and Xu (1998) for indoor simulation in FFD to investigate the distribution of airflow and temperature in the outdoor environment of four campus buildings, urban street canyons and an island with around 1500 buildings (Jandaghian, Mortezazadeh, & Wang, 2018; Katal, Mortezazadeh, & Wang, 2019; Mortezazadeh, & Wang, 2018). The zero-equation model overestimated the turbulence

dissipation in the area away from the building and could not provide accurate simulation results around the building, therefore it was not applicable in the outdoor environment. Because of the diversity of city terrains, the variety of building heights, and the complexity of building structures, outdoor airflow around buildings was extremely complicated. The flow scale of the outdoor environment might vary from millimeter to kilometer. Therefore, the turbulence models that worked indoors might not work outdoors. Mortezazadeh applied Smagorinsky model in FFD to simulate the flow and temperate distribution around a cylinder block, around a group of low-rise buildings and in the whole city of Montreal (Mortezazadeh, 2019; Mortezazadeh, & Wang, 2020). However, they only used one turbulence model for simulation and did not conduct the comparison of different turbulence models. Turbulence model played a vital role in computing accuracy and efficiency. There were many types of models, and each had advantages and disadvantages. Such as the constant coefficient in Smagorinsky model might cause errors and it could be avoided by using dynamic Smagorinsky model (Murakami, Iizuka, Ooka, 1999). The drawbacks of the above turbulence models were summarized in Table 1 (Wilcox, 2006). Therefore, it was of great importance to conduct the comparison of different turbulence models in FFD.

Table 1 Drawbacks of turbulence models

Turbulence model	Drawbacks
No turbulence model	It ignored turbulence pulsation and therefore caused errors.
RNG k-ε turbulence model	It could not reflect the anisotropy of turbulence; It took a long time to solve two partial differential equations to get eddy viscosity; It only provided an average quantity of the flow but no pulsation value.
Smagorinsky turbulence model	It could not reflect the anisotropy of turbulence; Model constant of it was not universal;
Dynamic Smagorinsky turbulence model	Dynamic calculation of the model coefficient was time-consuming.

Turbulence model was of great importance in airflow and concentration simulation. The turbulence model commonly used in FFD was RNG k-ε turbulence model, but it required to solve two partial differential equations to obtain eddy viscosity, which increased the computational time. This investigation implemented FFD with no turbulence model, Smagorinsky model and dynamic Smagorinsky model which calculated eddy viscosity without solving equation to reduce the computing time of this part and further improve the computing efficiency. We systematically evaluated the simulation result and computing time of FFD with some turbulence models through simulating cases of varying complexity. To make the evaluation results more referential, we also compared FFD with CFD, which was commonly used in outdoor environment simulation. The objective of the study is to assess the accuracy and computing efficiency of FFD with these turbulence models.

2. Research methods

This section provides a brief introduction of FFD and turbulence models used in this investigation.

2.1. Fast fluid dynamics

FFD solves the Navier-Stokes equations for an incompressible Newtonian fluid:

$$\rho \frac{\partial u_i}{\partial t} + \rho u_j \frac{\partial u_i}{\partial x_j} = -\frac{\partial p}{\partial x_i} + \mu \frac{\partial^2 u_i}{\partial x_j \partial x_j} + F_i \quad (1)$$

$$\frac{\partial u_i}{\partial x_i} = 0 \quad (2)$$

where i, j = 1, 2 and 3; x_i and x_j are spatial coordinates; u_i is the *i*th component of the velocity vector (m/s); t is time (s); p is pressure (Pa); ρ is density (kg/m^3); F_i is the *i*th component of the body forces (N/s·m^2); μ is the viscosity (N·s/m^2). The SIPC scheme (Guermond, Minev, & Shen, 2006) is applied to split Equation (1) into two discretized equations:

$$\rho \frac{u_i^* - u_i^n}{\Delta t} = -\frac{\partial p^n}{\partial x_i} - \rho u_j^n \frac{\partial u_i^*}{\partial x_j} + \mu \frac{\partial^2 u_i^*}{\partial x_j \partial x_j} + F_i \quad (3)$$

$$\rho \frac{u_i^{n+1} - u_i^*}{\Delta t} = -\frac{\partial (p^{n+1} - p^n)}{\partial x_i} \quad (4)$$

where u_i^n and u_i^{n+1} are the velocities at the previous and current time steps; u_i^* is the intermediate air velocity; p^n and p^{n+1} are the pressure at the previous and current time steps. Here u_i^* is obtained by solving Equation (3). The pressure projection method (Guermond, Minev, & Shen, 2006) is applied in resolving the coupled pressure and velocity. Substituting Equation (4) into Equation (1) yields:

$$\frac{\partial^2 (p^{n+1} - p^n)}{\partial x_i \partial x_i} = \frac{\rho}{\Delta t} \frac{\partial u_i^*}{\partial x_i} \quad (5)$$

where p^{n+1} is calculated by solving Equation (5). With u_i^* and p^{n+1}, Equation (4) can be used to obtain u_i^{n+1}.

The transport of scalars, such as gaseous contaminant concentrations, must be considered. After the velocity field has been obtained, transport equations for the other scalars are solved by:

$$\frac{\partial \phi}{\partial t} + u_j \frac{\partial \phi}{\partial x_j} = \Gamma \frac{\partial^2 \phi}{\partial x_j \partial x_j} + S \quad (6)$$

where ϕ is the transport scalar to be solved, Γ is the diffusive coefficient, and *S* is the source term.

2.2. Turbulence models

Equations (1) to (6) are Navier-Stokes equations for flow without turbulence. For turbulent flow around buildings, the RNG k-ε turbulence model (Yakhot, & Orszag, 1986) which solves two partial differential transport equations of k and ε to obtain turbulence viscosity μ_t is used. Smagorinsky model (Smagorinsky, 1963) filters the flow into large-scale flow and small-scale flow. The large-scale flow is calculated by the Navier-Stokes equations, and the effect of small-

scale flow is described by the Smagorinsky model. This model obtains the turbulence viscosity through calculating algebraic expression. In contrast, the dynamic Smagorinsky model (Germano, Piomelli, Moin, & Cabot, 1990) gets the coefficient C_s in the algebraic expression through dynamic calculation.

The transport equations of FFD without turbulence model and with the three turbulence models can be written in a general form:

$$\rho\frac{\partial\bar{\phi}}{\partial t}+\rho\bar{u_j}\frac{\partial\bar{\phi}}{\partial x_j}-\frac{\partial}{\partial x_j}\left[\Gamma_{\phi,eff}\frac{\partial\bar{\phi}}{\partial x_j}\right]=S_\phi \qquad (7)$$

where ϕ represents the given variable; $\Gamma_{\phi,eff}$ is the effective diffusion coefficient; S_ϕ is the source term. The bar over the variable indicates an average or filtered variable. Table 2 summarizes the coefficients and source terms of no turbulence model and the three turbulence models. Here u_i is the velocity component in the i direction (m/s); k is the kinetic energy of turbulence (m^2/s^2); ε is the dissipation rate of turbulence kinetic energy (m^2/s^3); p is the air pressure (Pa); μ_t is the eddy viscosity ($N{\cdot}s/m^2$); G_k is the turbulence production for k ($N/s{\cdot}m^2$); S is the rate of the strain (1/s); τ_{ij}^s is the subgrid scale stress (N/m^2); L_{ij} and M_{ij} are the resolved stress tensor (m^2/s^2).

Table 2 Coefficients and source terms

Turbulence model	ϕ	$\Gamma_{\phi,eff}$	S_ϕ	Constant and coefficients
No turbulence model	u_i	μ	$-\partial p/\partial x_i$	—
RNG k-ε	u_i k ε	$\mu+\mu_t$ $\mu+\mu_t/\sigma_{k,t}$ $\mu+\mu_t/\sigma_{\varepsilon,t}$	$-\partial p/\partial x_i$ $G_k-\rho\varepsilon$ $C_{\varepsilon1}G_k\varepsilon/k-C_{\varepsilon2}\rho\varepsilon^2/k$	$\mu_t=C_\mu\rho\frac{k^2}{\varepsilon};\ G_k=\mu_tS^2;\ S=\sqrt{2S_{ij}S_{ij}};$ $S_{ij}=\frac{1}{2}\left(\frac{\partial\bar{u_i}}{\partial x_j}+\frac{\partial\bar{u_j}}{\partial x_i}\right);\ C_{\varepsilon1}=1.44;$ $C_{\varepsilon2}=1.92;\ C_\mu=0.09;$ $\sigma_{k,t}=1;\sigma_{\varepsilon,t}=1.3;$
Smagorinsky	u_i	$\mu+\mu_t$	$-\frac{\partial\bar{p}}{\partial x_i}-\frac{\partial\tau_{ij}^s}{\partial x_j}$	$\tau_{ij}^s=\mu_t\left(\frac{\partial\bar{u_i}}{\partial x_j}+\frac{\partial\bar{u_j}}{\partial x_i}\right)+\frac{1}{3}\rho\tau_{kk}^s\delta_{ij};$ $\mu_t=\rho(C_s\Delta)^2\sqrt{2\bar{S_{ij}}\,\bar{S_{ij}}};\ C_s=0.18$
Dynamic Smagorinsky	u_i	$\mu+\mu_t$	$-\frac{\partial\bar{p}}{\partial x_i}-\frac{\partial\tau_{ij}^s}{\partial x_j}$	$\tau_{ij}^s=\mu_t\left(\frac{\partial\bar{u_i}}{\partial x_j}+\frac{\partial\bar{u_j}}{\partial x_i}\right)+\frac{1}{3}\rho\tau_{kk}^s\delta_{ij};$ $\mu_t=\rho(C_s\Delta)^2\sqrt{2\bar{S_{ij}}\,\bar{S_{ij}}},C_s=\sqrt{\frac{\langle L_{ij}M_{ij}\rangle}{\langle M_{ij}M_{ij}\rangle}}$

This investigation has implemented FFD without turbulence model and with the three turbulence models in Open Field Operation and Manipulation (OpenFOAM) (Weller, Tabor, Jasak, & Fureby, 1998), an open-source program. CFD with RNG k-ε turbulence model is conducted with the use of a commercial program, ANSYS Fluent 14.0 (ANSYS, 2011). Some studies on comparison of different CFD codes showed that OpenFOAM had different performance compared with FLUENT with different numerical settings, such as different solution method, solver type and time step etc. (Welahettige, & Vaagsaether, 2016). However, when the numerical settings of both CFD codes were the same, they gave similar results

(Lysenko, Ertesvåg, & Rian, 2013; López, Nicholls, Stickland, & Dempster, 2015). This investigation used the same settings for both software to conduct the simulation.

3. Case setup

3.1. Case description

To evaluate the accuracy and computational efficiency of FFD and CFD with different turbulence models, this study tested them on several outdoor cases of varying complexity, including a single building, several buildings and an array of buildings, for which experimental data were available in the literature.

The single-building case was a classical benchmark case for outdoor wind environment simulation (Tanaka, Yoshie, & Cheng, 2006). The experiment was conducted in a wind tunnel at the Tokyo Polytechnic University. The model building had a height (H) of 200 mm, a width of 100 mm and a depth of 100 mm, as shown in Fig. 1(a). There was a point source of tracer gas, which was a hole of two millimeters in diameter on the floor, located 50 mm leeward of the model building. The tracer gas, ethylene, was released from the hole at a flow rate of q = 5.83 x 10^{-6} m^3/s. Measuring locations were on the vertical center plane, as shown in Fig. 1(b). The inlet boundary conditions of velocity and turbulence kinetic energy measured in the experiment were shown in Fig. 2.

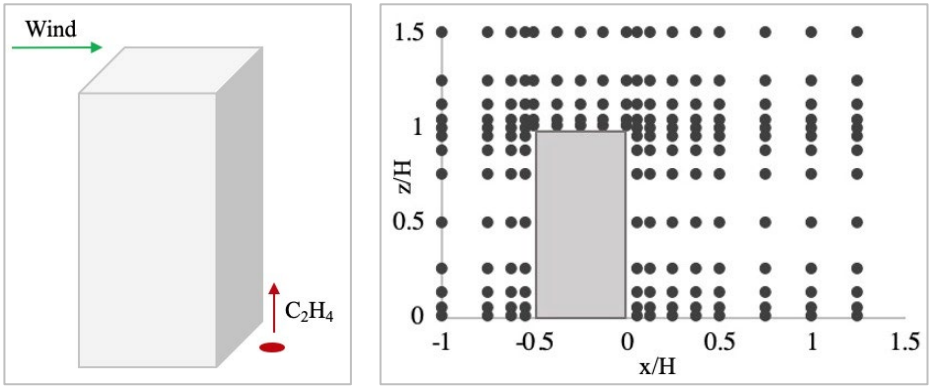

(a) (b)

Fig. 1. (a) Geometric configuration of the single building and (b) measurement point locations for velocity and concentration.

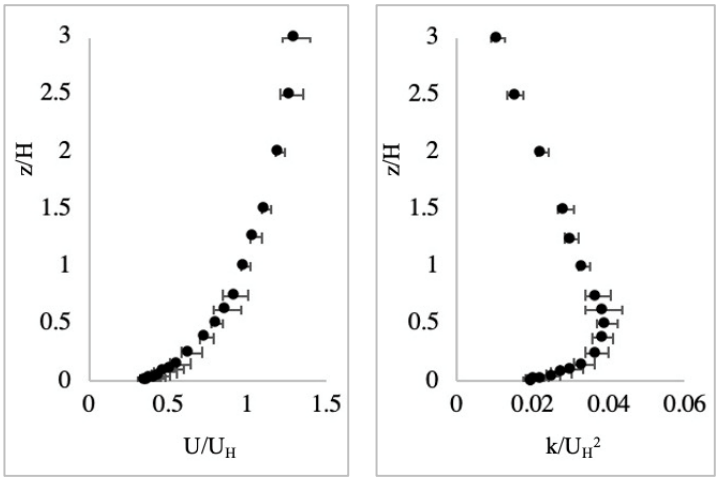

(a) (b)

Fig. 2. Inflow profiles of (a) velocity and (b) turbulence kinetic energy. Note: U_H was the inflow velocity at the building height.

The three-building case as shown in Fig. 3(a) was from Chavez et al.(Chavez, Hajra, Stathopoulos, & Bahloul, 2011). They conducted the wind tunnel experiment in the open-circuit, boundary layer wind tunnel at Concordia University. The dimensions of the buildings were shown in Table 3, and they were constructed on a 1:200 scale. A mixture of SF_6 and nitrogen with a concentration of 10 ppm was released from a stack at a speed of 18.3 m/s. The height of the stack was 0.005m and the diameter was 0.003m. The stack location was 0.1 m from the upwind edge of B1 and 0.125 m from the lateral edges. The inlet boundary conditions of the domain were summarized in Table 4. Measurements of the SF_6 concentration were conducted using receptors located centrally on the rooftop of the center building and spaced 0.025 m apart and 0.125 m from the lateral edges, as shown in Fig. 3(b).

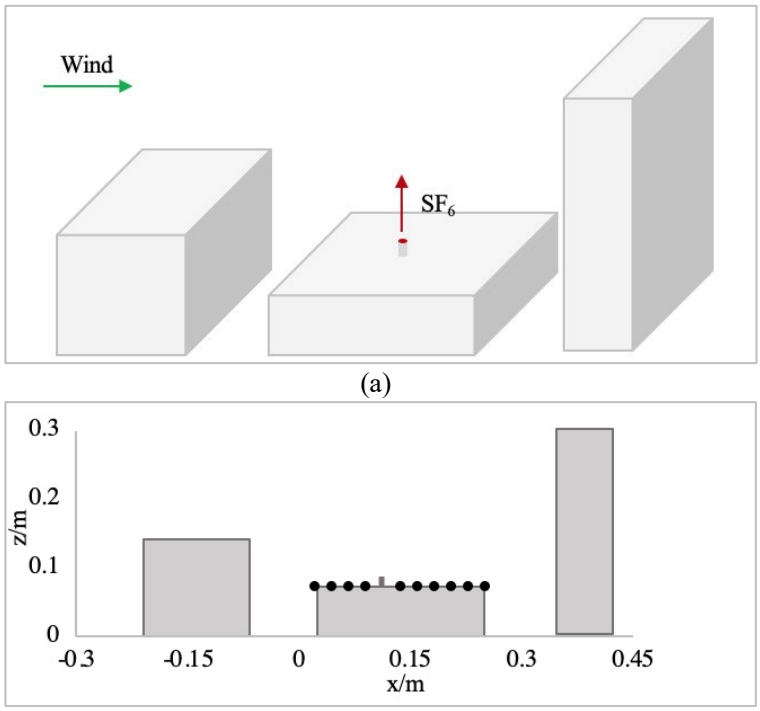

Fig. 3. (a) Geometric configuration of the three buildings and (b) measurement locations for SF_6 concentration.

Table 3 Dimensions of the three buildings

Building	Height (m)	Width (m)	Length (m)
B1	0.075	0.25	0.25
B2	0.15	0.25	0.15
B3	0.27	0.22	0.075

Table 4 Summary of inflow boundary conditions

Velocity (m/s)	Turbulence kinetic energy (m^2/s^2)	Dissipation rate
$U = U_H(\frac{z}{z_0})^{0.33}$	$k = 0.5(I_U U)^2$	$\varepsilon = (\frac{U\kappa}{\ln(z/z_0)})^3/\kappa z$

Note: I_U represented the turbulence intensity values; κ was the von Karman constant, and z_0 was the roughness length (m).

The last case was an array of buildings. The airflow and pollutant dispersion were measured in a finite array of rectangular building models in the Blasius wind tunnel at the University of Hamburg (Leitl, & Schatzmann, 2010). The building models were constructed on a reduced scale of 1:200. The experimental model consisted of 3 × 7 array of buildings with dimensions of 0.1 m × 0.15 m × 0.125 m, as shown in Fig. 4(a). The pollutant sources were simulated by CO_2 tracer gas that was uniformly released from the four sources located on the leeward wall of the source building at a constant velocity of 0.025 m/s. Measurement points were located on the horizontal plane with z = 0.0075 m and the vertical center plane, as shown in Fig. 4(b) and Fig. 4(c). Table 5 summarized the inlet boundary conditions of the domain.

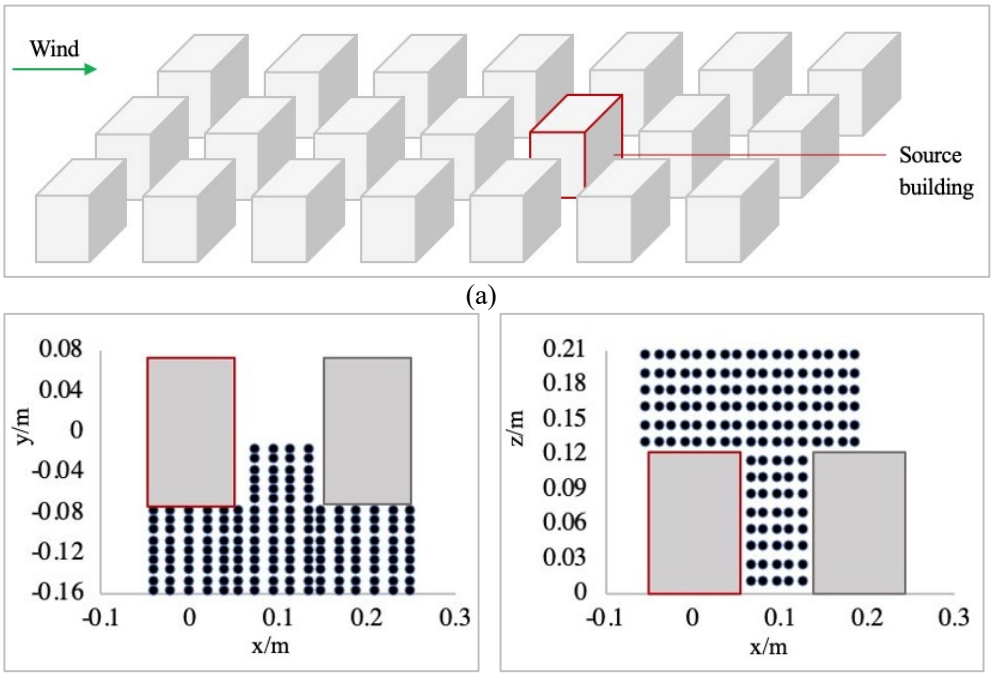

Fig. 4. (a) Geometric configuration of the array of buildings, (b) measurement locations for CO_2 concentration and (c) measurement locations for velocity

Table 5 Summary of inflow boundary conditions.

Velocity	Turbulence kinetic energy	Dissipation rate
$U = \frac{U^*}{\kappa}\ln(\frac{z+z_0}{z_0})$	$k = \sqrt{C_1 \ln(z+z_0) + C_2}$	$\varepsilon = \frac{U^*\sqrt{C_\mu}}{\kappa(z+z_0)}\sqrt{C_1 \ln(z+z_0) + C_2}$

Note: The coefficients were determined by experimental data. z_0 = 0.00075 m, U^*= 0.4078 m/s, C_1 = 0.025, C_2 = 0.41, the Von Karman constant κ = 0.4187, and C_μ = 0.069.

3.2. CFD/FFD model setup

For the size of the computational domain, the blockage ratio should be below 3% to reduce the influence of lateral walls on the region of interest (Tominaga, Mochida, Yoshie, & Kataoka, 2008). As shown in Fig. 5, in the three cases, all the buildings were included in the building area. The lateral, inlet and top boundary were set at a distance of 5H from the building area (Franke, & Baklanov, 2007), where H was the height of the tallest building in the area. A distance of 15H was set between the outlet boundary and the building, and it was sufficient for flow to develop. The calculated blockage ratios for the three cases were 0.79%, 1.31% and

1.32%, respectively, meeting the requirement of less than 3% (Tominaga, Mochida, Yoshie, & Kataoka, 2008).

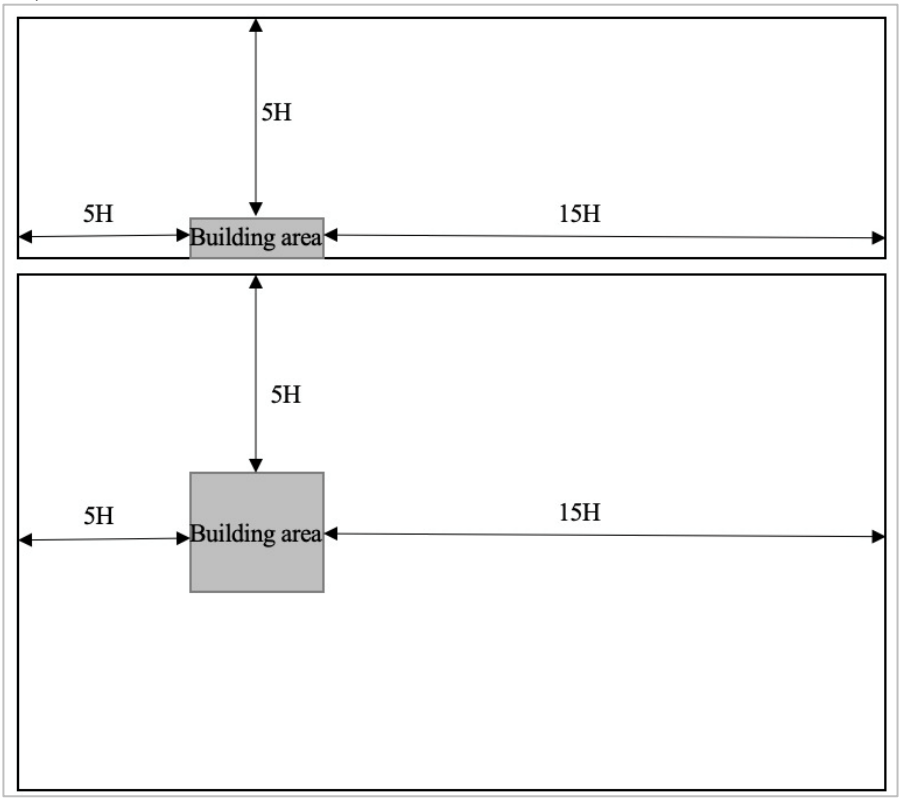

Fig. 5. Computational domain: side view and top view of the three cases.

The grid was meshed according to the guidelines (Tominaga et al., 2008; Franke, & Baklanov, 2007; Blocken, 2015; Yoshie et al., 2005). The grid stretching ratio was set below 1.3 in regions of high gradient to limit the truncation error. Three grid systems, with coarse, medium and fine unstructured tetrahedral grid, were constructed in each case for grid independence and the minimum refined ratio for two consecutive grids was 3.375, which meant that the grid was refined by 1.5 times in each dimension. The grid independence test was illustrated in detail in Appendix A. Fig. 6 demonstrated the resulting meshes of 0.372 million, 0.973 million and 1.503 million, respectively.

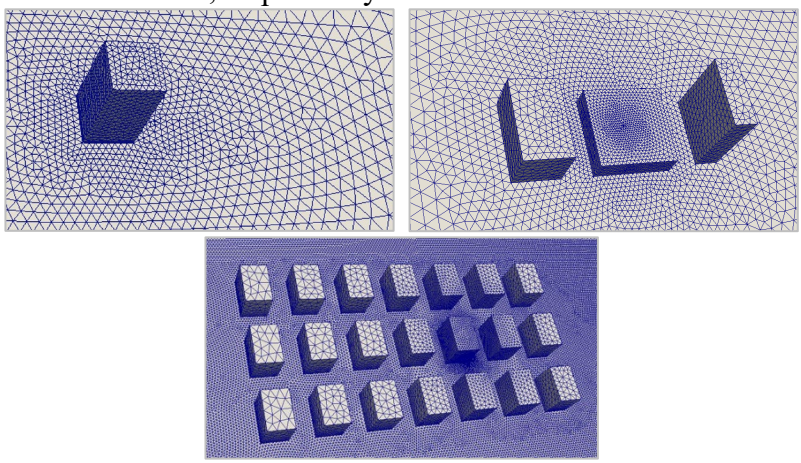

(a) (b) (c)

Fig. 6. The meshes for (a) the single building, (b) the three buildings, (c) the array of buildings

Fig. 7 showed the boundary conditions in the simulations. The ground and the building surfaces were modeled as non-slip wall, and the roughness length of ground was calculated using experimental data. The sides and the top of the computational domain were set as symmetry. The inlet of the domain and the pollutant exhaust outlet were set as velocity inlet. Inflow boundary conditions were set by interpolation of experiment data or formula calculation according to the case introduction in section 3.1. The outlet was specified as outflow to generate a fully developed flow.

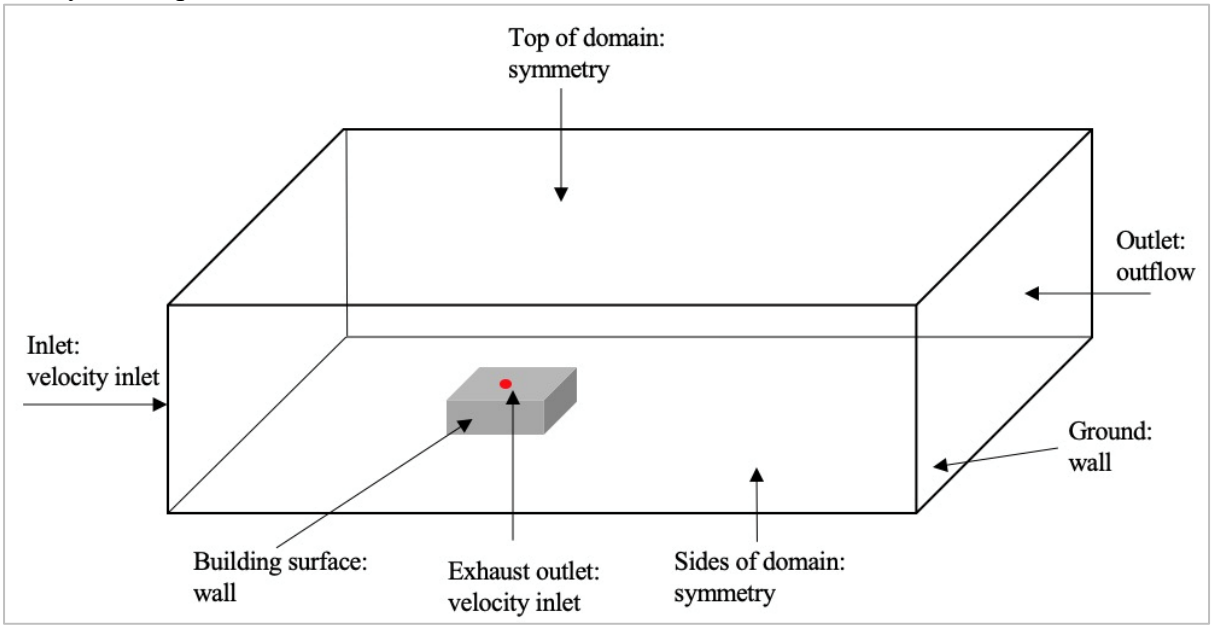

Fig. 7. Boundary conditions of the three cases

The governing transport equations were solved by means of the finite volume method. The discretization schemes for the convection and viscous terms of the governing equations were second-order discretization scheme in CFD and were linearUpwind discretization scheme in FFD. Both schemes considered the effect of the flow direction and were second-order precision. The results were considered converged when the residuals for all the independent parameters reached 10^{-5}. To ensure stable calculation, the time step was set according to the principle that the mean Courant–Friedrichs–Lewy (CFL) number was less than one. The Courant number was defined as (Gnedin, Semenov, & Kravtsov, 2018):

$$CFL = \frac{\Delta t|U|}{\Delta x} \tag{8}$$

where Δx was the mesh size and U was the velocity at the cell.

To eliminate the influence of the initial condition, the results for the first 2τ time were not used. Here τ was the time required for the airflow to pass through the domain once, which was called the time constant. The sampling length was 5τ to ensure accurate time-average result.

3.3. Evaluation

We compared the total time to evaluate the computing efficiency. To identify the reason for different computing time, we also compared the time for solving P, U and C equations and calculating eddy viscosity μ_t.

We used the normalized root mean square error (NRMSE) to quantitatively evaluate the accuracy of simulation results, which was defined as (Wang, & Zhai, 2012):

$$NRMSE(P,M) = \sqrt{\frac{\sum_{i=1}^{n} \delta_{pm}\left(|P(i) - M(i)| - e(i)\right)^2}{\sum_{i=1}^{n} M(i)^2}} \quad (9)$$

$$\delta_{pm} = \begin{cases} 1, & |P(i) - M(i)| \geq e(i) \\ 0, & |P(i) - M(i)| < e(i) \end{cases} \quad (10)$$

where $P(i)$ was the simulated value; $M(i)$ was the measured value; $e(i)$ was the experimental uncertainty.

4. Results

This section presented the performance assessment of FFD and CFD methods with different turbulence models in terms of accuracy and computing time of the three cases. For the sake of accuracy, we used experimental data from the literature as the benchmark.

4.1. Single-building case

Fig. 8 portrayed the normalized scalar velocity contour with the mark of the recirculation zone on the central vertical plane obtained by simulations and experiment. The reattachment length of them were summarized in Table 6. The reattachment length in the result of FFD without turbulence model was much longer than that of the experiment. The possible reason was that the model did not consider the turbulence viscosity, and the total viscosity was small, so the forward airflow was less affected by the flow in other directions. Excessive forward flow caused the long recirculation zone. In the simulation of FFD and CFD with the RNG k-ε turbulence model, the reattachment zone on the roof was connected to the recirculation zone behind the building. The reattachment length behind the building was over-predicted because the periodic fluctuation there was not reproduced. The momentum diffusion was under-predicted, so the velocity of the recirculation zone was also overestimated. The overestimation of the reattachment length was also observed in the result of the Smagorinsky model. A possible explanation was that the model constant was unsuitable here. The dynamic Smagorinsky model improved the result by dynamically calculating the model constant.

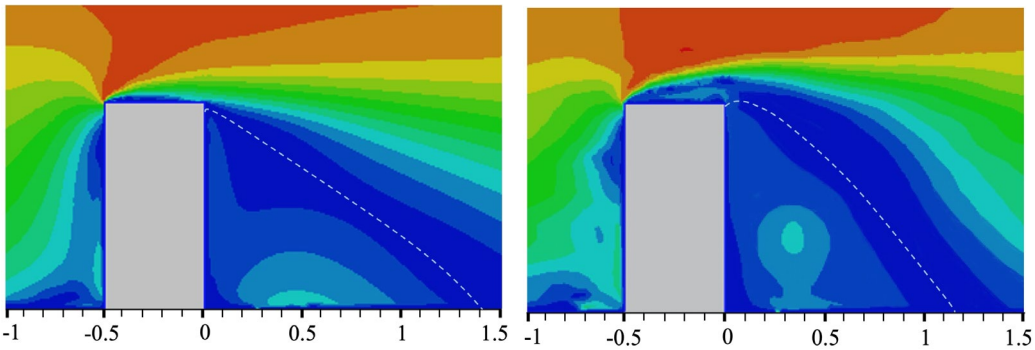

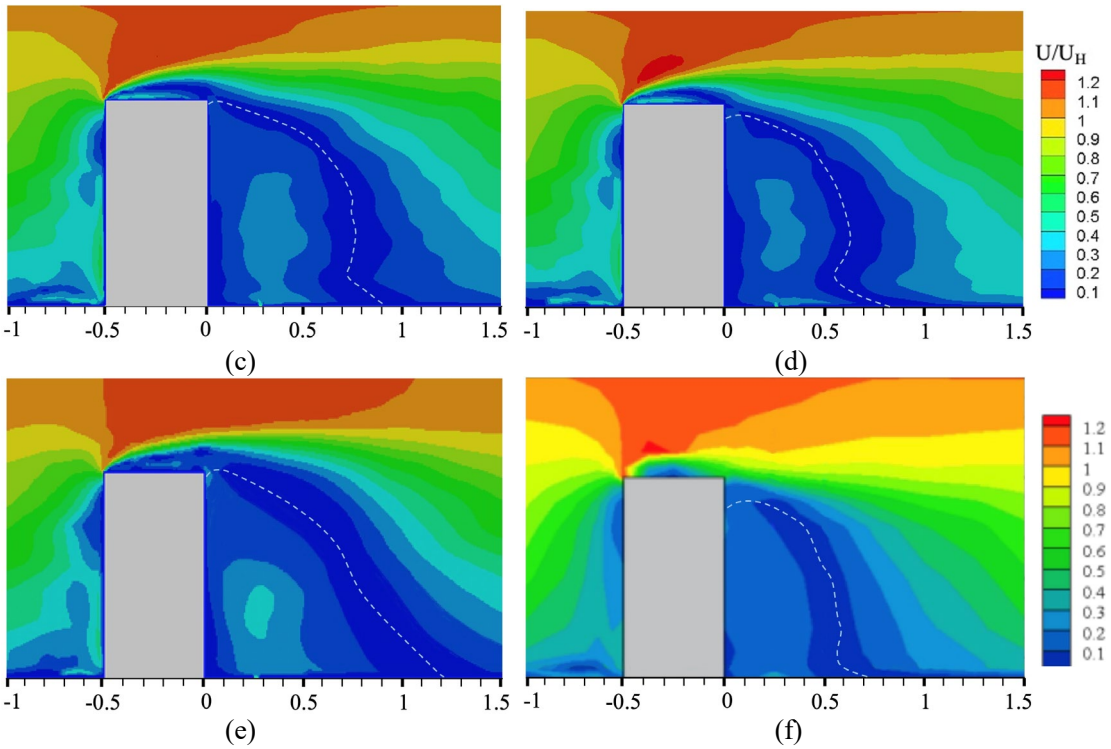

Fig. 8. Contours of normalized scalar velocity simulated by (a) FFD without turbulence model, (b) FFD with the RNG k-ε turbulence model, (c) FFD with the Smagorinsky model, (d) FFD with the dynamic Smagorinsky model, (e) CFD with the RNG k-ε turbulence model and (f) the corresponding experimental data.

Table 6 Summary of reattachment length.

Simulation and experiment	FFD + No turbulence model	FFD+ RNG k-ε turbulence model	FFD + Smagorinsky model	FFD + Dynamic Smagorinsky model	CFD+RNG k-ε turbulence model	Experiment
reattachment length	1.42H	1.15H	0.91H	0.83H	1.22H	0.71H

Fig. 9 depicted the normalized concentration contour on the central vertical plane obtained by simulations and experiment. The concentration on the leeward side of the building was overestimated in the contour produced by FFD without turbulence model. The reason for this phenomenon might be that the reverse velocity at the pollution source was too large, causing the pollutant to concentrate on the leeward side of the building. In the results of FFD and CFD with RNG k-ε turbulence model, the dispersion of pollutant was over-predicted on account of the overestimated recirculation zone. Because the reattachment zone on the roof was connected to the recirculation zone behind the building, pollutants spread to the roof, leading to an overestimation of the concentration there. For the same reason, the concentration on the roof was also over-predicted in the result simulated by the Smagorinsky model. By dynamically calculating model coefficient, the results in the dynamic Smagorinsky model were improved. Since the recirculation zones on the roof and behind the building were not connected, the pollutant did not spread to the roof, and the overestimation of the concentration in the recirculation zone was also reduced.

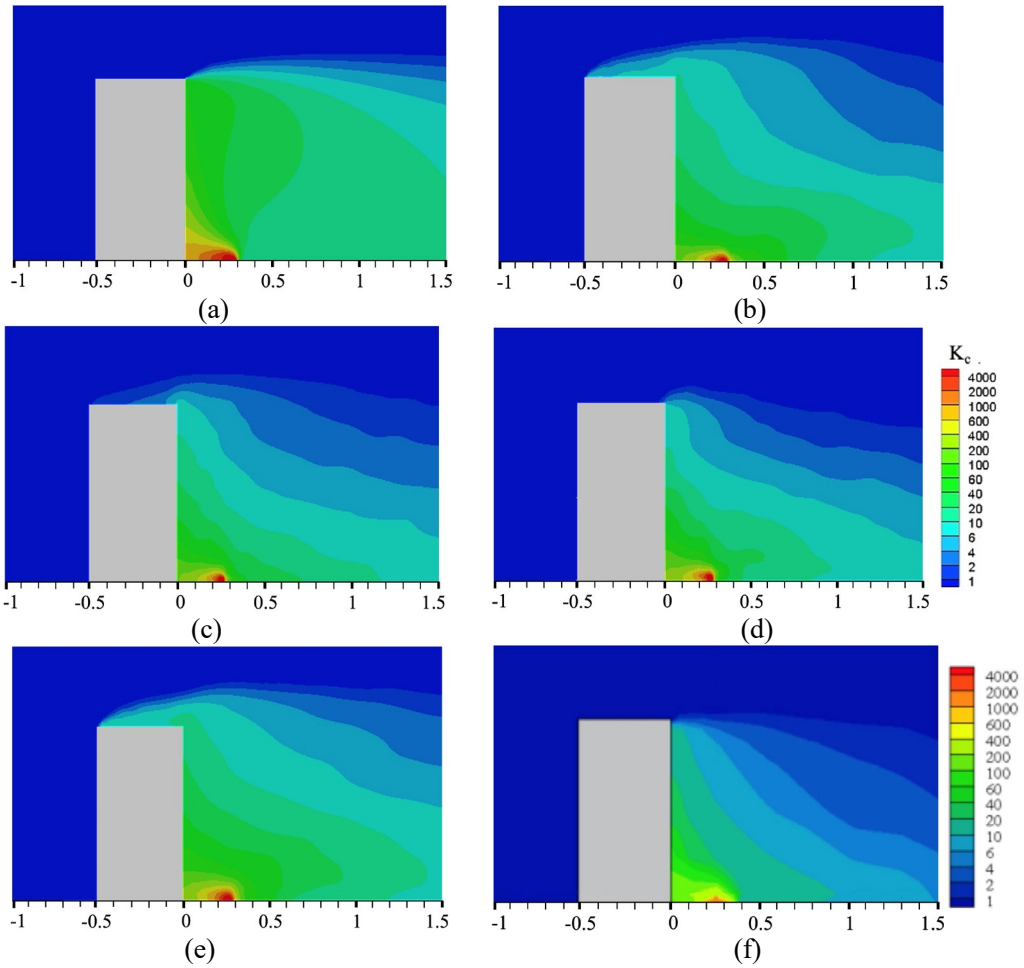

Fig. 9. Contours of normalized concentration K_c simulated by (a) FFD without turbulence model, (b) FFD with the RNG k-ε turbulence model, (c) FFD with the Smagorinsky model, (d) FFD with the dynamic Smagorinsky model, (e) CFD with the RNG k-ε turbulence model and (f) the corresponding experimental data. Note: The concentration was in a non-dimensional form, expressed as $K_c = \frac{CU_HH^2}{C_{gas}Q}$, where C was the gas concentration (ppm); C_{gas} was the released tracer-gas concentration (ppm); U_H was the reference wind velocity (m/s) measured at height H; H was the building height (0.2 m) and Q was the released gas emission (m^3/s).

Fig. 10 showed the distribution of normalized scalar velocity and concentration on a vertical line in the recirculation zone behind the building. In the velocity profile, the result without turbulence model was the worst, the other four simulation results had similar overall distributions and a better agreement with the measurements. The result of the dynamic Smagorinsky model was the closest to the experiment near the ground, which also corresponded to the minimum reattachment length of it in the velocity contour. In the concentration profile, the simulated values of the five sets were all larger than the measured, especially in the result of FFD without turbulence model. This corresponded to the overestimation of the concentration in the recirculation zone in the contour. The results of CFD and FFD with RNG k-ε turbulence model was similar. Compared with Smagorinsky model, the overestimation of concentration was improved in the result of dynamic Smagorinsky model. It meant that the constant coefficient in Smagorinsky model was unsuitable here, and dynamic calculation of it could improve results.

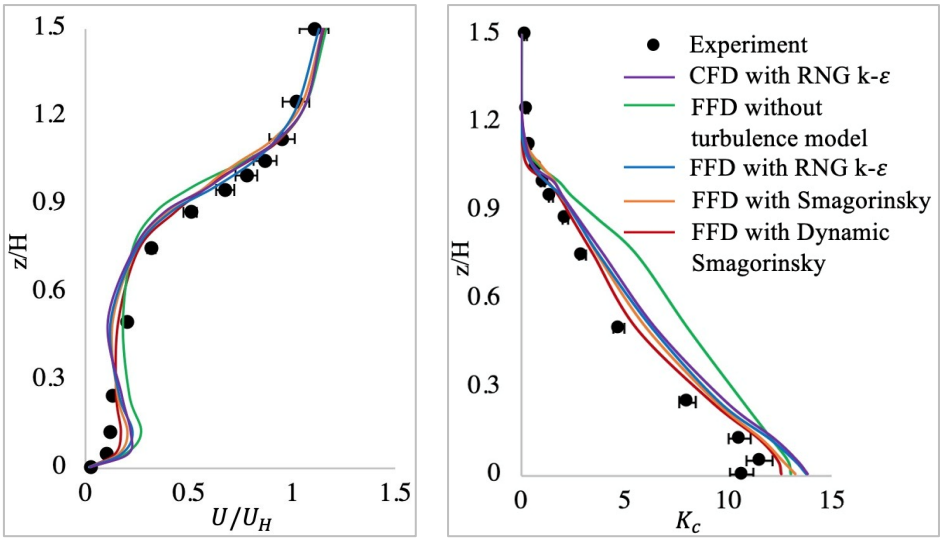

(a) (b)

Fig. 10. Comparison of (a) the normalized scalar velocity and (b) the normalized concentration between the five simulations and the measured values at x = 0.75H on the center vertical plane

The above were all qualitative comparisons of the simulation accuracy. Next, the normalized root mean square error (NRMSE) was used to quantitatively evaluate the results. As shown in Table 7, the velocity errors in the simulations were small, while the concentration errors were larger. This showed that the turbulence diffusion had a greater influence on the concentration distribution and a smaller influence on the velocity distribution. The dynamic Smagorinsky model performed best, FFD without turbulence model was the least accurate, and the accuracy of the other three methods were between the first two. In general, the difference between the errors of those methods was not large. Hence, the accuracy of those turbulence models were not much different in a case with simple geometry.

Table 7 Summary of simulation accuracy.

Turbulence model	CFD+RNG k-ε turbulence model	FFD + No turbulence model	FFD+ RNG k-ε turbulence model	FFD + Smagorinsky model	FFD + Dynamic Smagorinsky model
Velocity NRMSE	10.23%	14.95%	9.89%	8.44%	7.76%
Concentration NRMSE	23.01%	30.89%	22.48%	21.52%	19.63%

4.2. Three buildings case

Fig. 11 displayed the scalar velocity contour on the central vertical plane simulated by FFD and CFD methods. We also compared the five simulation results with that of other researches which also simulated the three-building case and conducted wind tunnel experiment (Chavez, Hajra, Stathopoulos, & Bahloul, 2011; Hajra, Stathopoulos, & Bahloul, 2013; Chavez, Stathopoulos, & Bahloul, 2015; Bahloul, Stathopoulos, Hajra, & Chavez, 2014). All the simulation results had a recirculation zone on the roof of the middle building, which was in the wake region of the upwind building. However, FFD without turbulence model over-predicted the size of the recirculation zone. Moreover, the results of the five methods all had a downward airflow on the windward side of the right building, which was caused by the obstruction effect of the building on the forward flow. FFD without turbulence model overestimated the velocity on the windward side. The reason for higher velocity on the windward was that it ignored the velocity fluctuation, thus underestimating the dissipation of kinetic energy, which led to an

overestimation of velocity. The results of the dynamic Smagorinsky model and Smagorinsky model were similar.

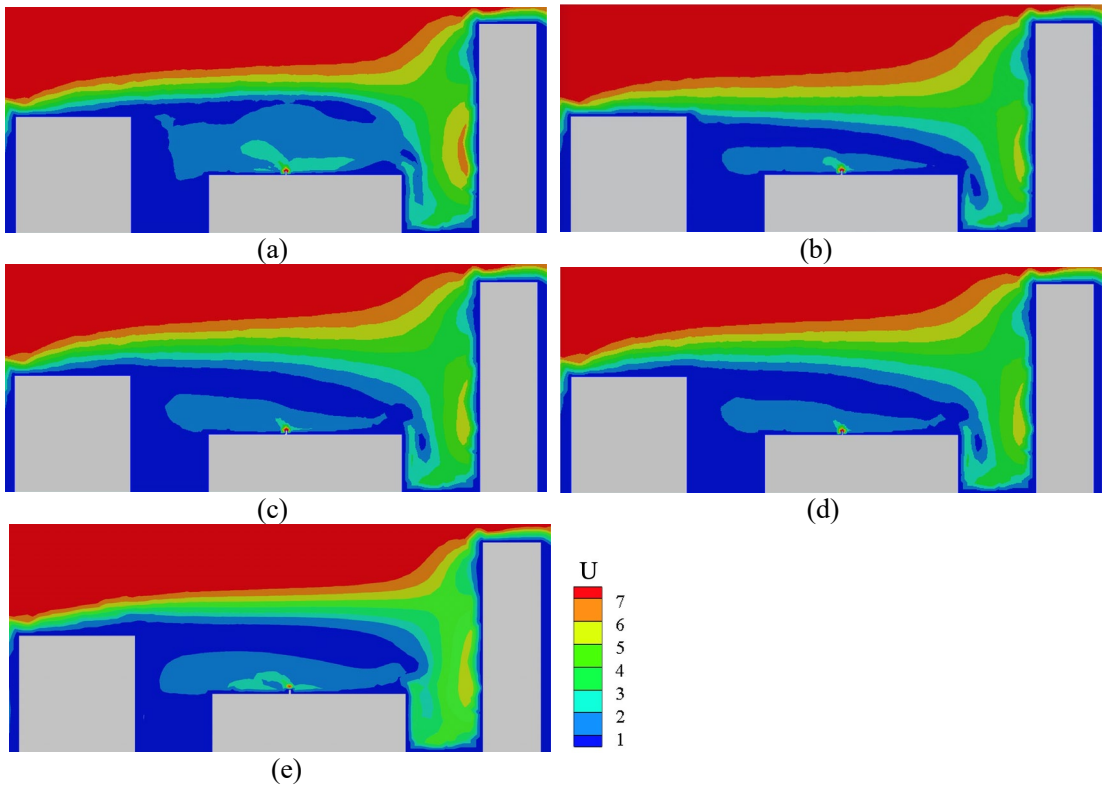

Fig. 11. Contours of scalar velocity simulated by (a) FFD without turbulence model, (b) FFD with the RNG k-ε turbulence model, (c) FFD with the Smagorinsky model, (d) FFD with the dynamic Smagorinsky model and (e) CFD with the RNG k-ε turbulence model

Fig. 12 depicted the concentration contour on the central vertical plane obtained by simulations. The pollutant was concentrated on the area between the buildings, because of the recirculation zone generated by the left building in combination with the obstruction effect of the right building. Due to the reverse velocity near the pollution source, the pollutant spread to the area between the middle building and the left building. On the windward side of the right building, the concentration was low because of the horizontal airflow which brought clean air down across the surface when it reached the building. We also compared the five simulation results with that of another research which also simulated the three-building case and conducted wind tunnel experiment (Chavez, Hajra, Stathopoulos, & Bahloul, 2011; Hajra, Stathopoulos, & Bahloul, 2013; Chavez, Stathopoulos, & Bahloul, 2015; Bahloul, Stathopoulos, Hajra, & Chavez, 2014). In the simulation result of FFD without turbulence model, the concentration in the center of the recirculation zone was too low, and around was high. This was because it ignored the turbulence fluctuation. The pollutants diffused along with the flow, which led to the excessive concentration in the periphery of the recirculation zone, and low concentration in the center. The concentration between the left and middle buildings simulated by the RNG $k-\varepsilon$ turbulence model was over-predicted. The difference between the two Smagorinsky models was that the pollutants diffusion range of dynamic Smagorinsky model was wider. This meant that the constant coefficient of Smagorinsky model was too small, and it became bigger by dynamic calculation.

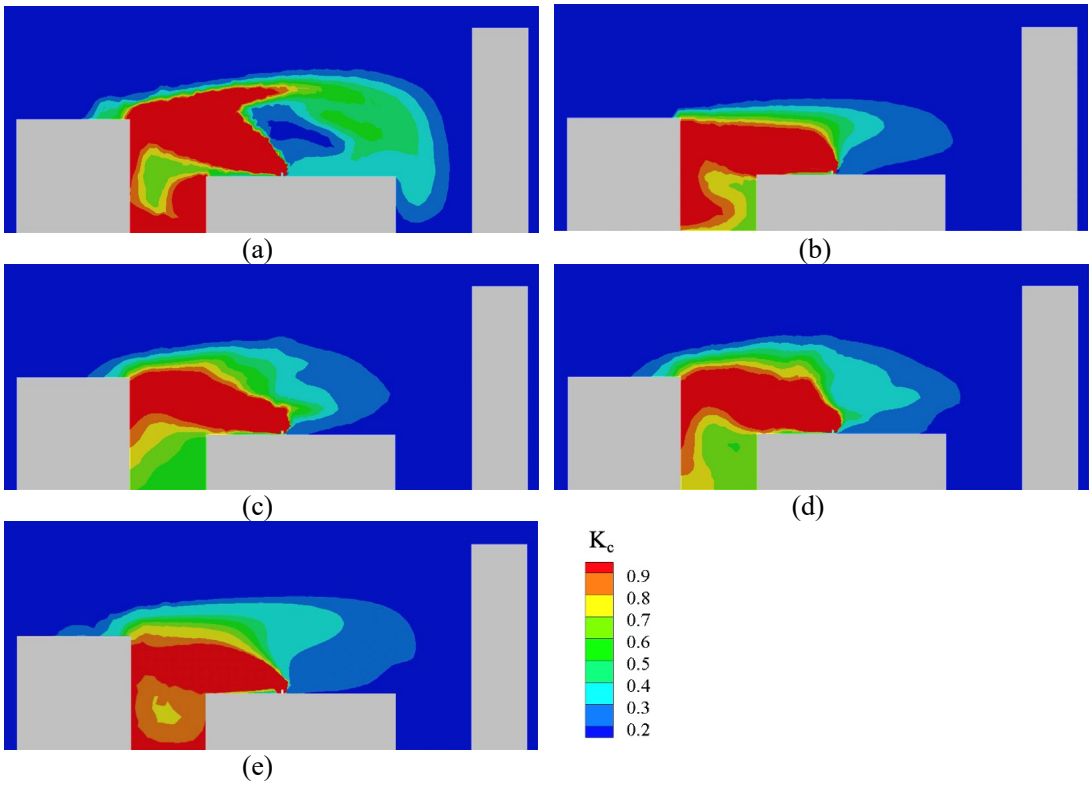

Fig. 12. Contours of normalized concentration K_c simulated by (a) FFD without turbulence model, (b) FFD with the RNG k-ε turbulence model, (c) FFD with the Smagorinsky model, (d) FFD with the dynamic Smagorinsky model and (e) CFD with the RNG k-ε turbulence model. Note: The concentration was in a non-dimensional form, expressed as $K_c = \frac{CU_H H^2}{C_{gas} Q}$, where C_{gas} was the contaminant mass fraction in the exhaust (ppm); C was the contaminant mass fraction at the location (ppm); Q was the flow rate at the exhaust (m^3/s); U_H was the wind velocity at the height of the upwind building (m/s) and H was the upwind building height (m).

Fig. 13 showed the pollutant concentration distribution on the central horizontal line on the middle building roof. In the result simulated by FFD without turbulence model, the concentration was much lower than the measured data at the front of the roof. Because the turbulence diffusion was underestimated, and the pollutants flowed away without spreading to the front of the roof. The simulation results of the other four sets of simulations were similar, and they all underestimated the concentration.

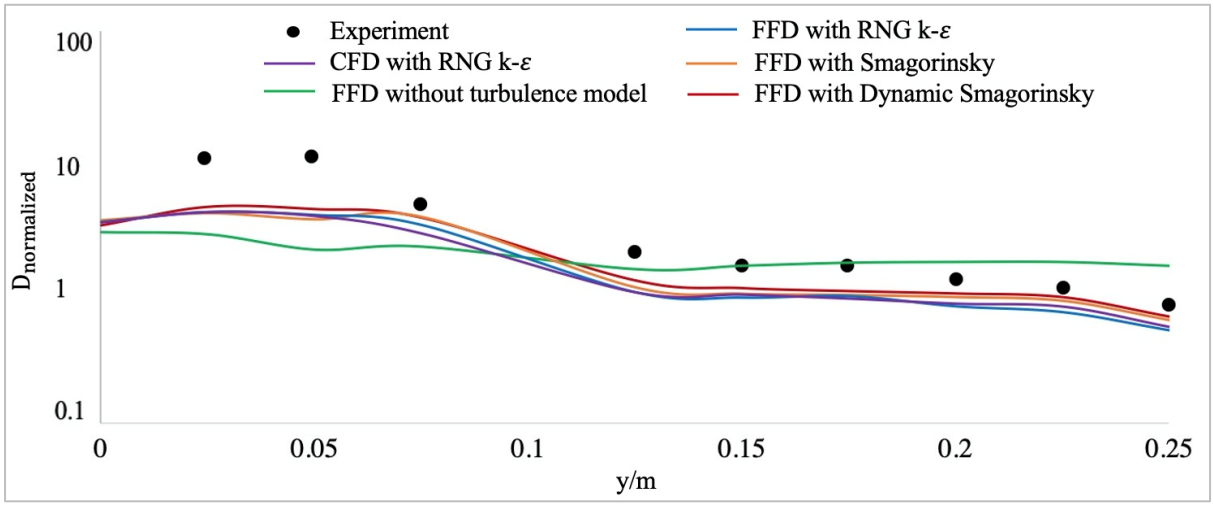

Fig. 13. Comparison of the normalized concentration between the five simulation results and the measured values on the central horizontal line on the roof

Table 8 provided the concentration errors of the five simulations along the central horizontal line on the middle building roof. The simulation error of FFD without turbulence model was the largest. Because this model treated the flow as laminar, and the pollutants diffusion was underestimated. Only small difference existed between the simulation results of CFD and FFD with RNG k-ε turbulence model, indicating that the accuracy of FFD and CFD were similar. The dynamic Smagorinsky model had the smallest error and therefore was the most accurate model in three buildings case.

Table 8 Summary of simulation accuracy.

Turbulence model	CFD+RNG k-ε turbulence model	FFD + No turbulence model	FFD+ RNG k-ε turbulence model	FFD + Smagorinsky model	FFD + Dynamic Smagorinsky model
Concentration NRMSE	72.57%	90.90%	71.69%	69.13%	67.57%

4.3. Case with an array of buildings

Fig. 14 compared the simulated concentration contour on the horizontal plane Z = 0.0075 m with the corresponding experimental data. The comparison showed that FFD and CFD with RNG k-ε turbulence model overestimated the dispersion of pollution due to the over-prediction of turbulence dissipation. Smagorinsky model underestimated the concentration. The dynamic Smagorinsky model improved the result through dynamically calculating the model coefficient. Surprisingly, the simulation without turbulence model also provided relatively accurate results. The possible reason was that FFD without turbulence model was equivalent to directly solve the Navier-Stokes equation, and the grid near the pollution source was small, which was close to the scale required to directly solve the equation. Therefore, the simulation result was relatively accurate.

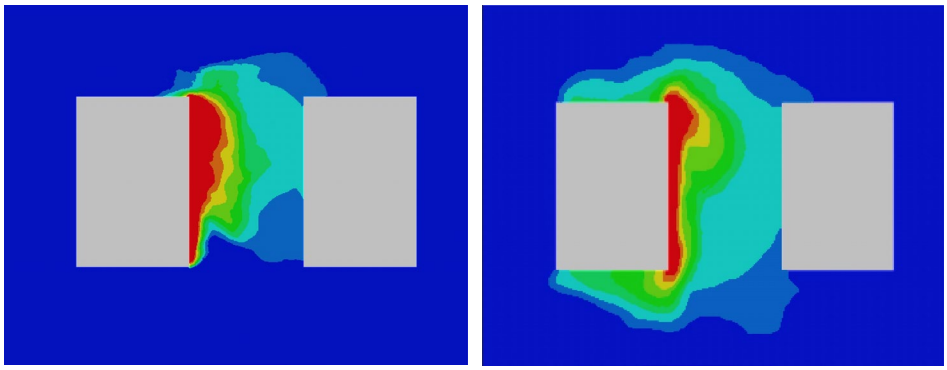

(a) (b)

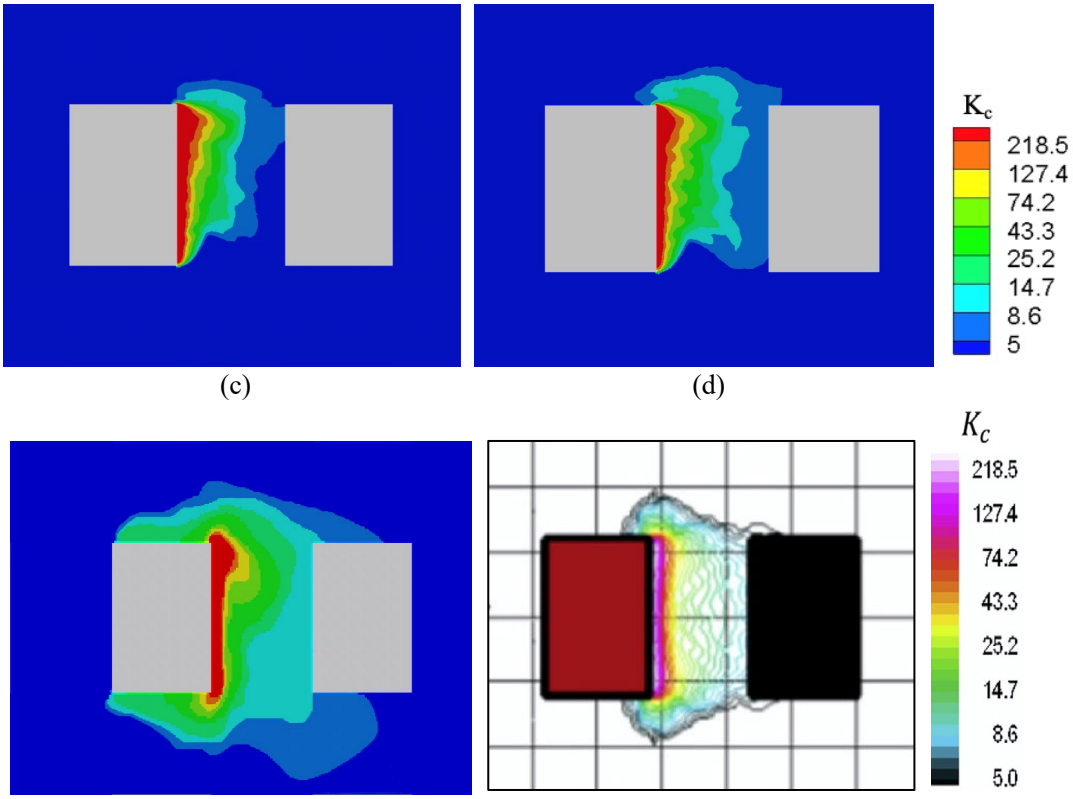

Fig. 14. Contours of normalized concentration K_c simulated by (a) FFD without turbulence model, (b) FFD with the RNG k-ε turbulence model, (c) FFD with the Smagorinsky model, (d) FFD with the dynamic Smagorinsky model, (e) CFD with the RNG k-ε turbulence model and (f) the corresponding experimental data. Note: The concentration value was normalized to a non-dimensional form, expressed as $K_c = \frac{CU_H H^2}{C_{gas} Q}$, where C was the measured concentration (ppm); C_{gas} was the concentration (ppm) at the source; U_H was the reference wind velocity (m/s) measured at 0.66 m; H was the building height (0.125 m) and Q was the flow rate of the source emission (m^3/s).

Fig. 15 compared the simulated velocity in z-direction on a vertical line and the normalized pollutant concentration in y-direction on a horizontal line with the corresponding experimental data. The velocity profile of the five simulations were close to each other. FFD and CFD with RNG k-ε turbulence model over-predicted the pollutant concentration. As explained above, it was caused by the over-valuation of turbulence dispersion. The Smagorinsky model under-predicted the concentration, which corresponded to the concentration contour. The dynamic Smagorinsky model performed the best. The simulation of FFD without turbulence model also had a relatively high accuracy.

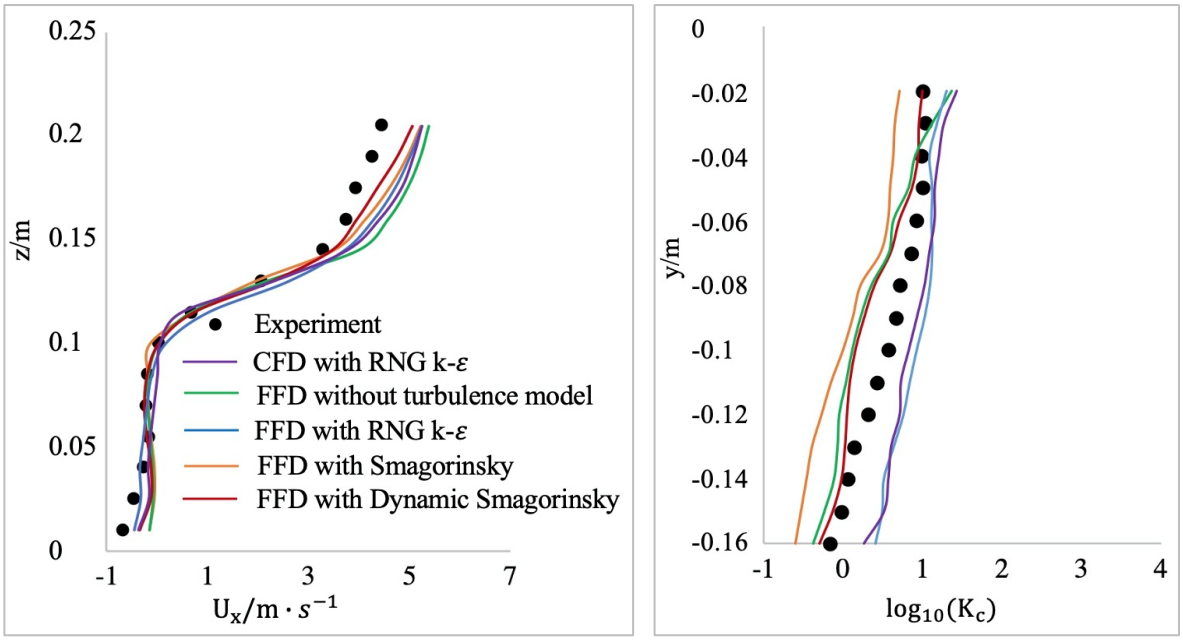

(a) (b)

Fig. 15. Comparison between the simulated (a) normalized velocity in *z*-direction on a vertical line and (b) normalized concentration in *y*-direction on a horizontal line and the corresponding experimental data.

Table 9 showed the statistical velocity errors of FFD and CFD on the central vertical plane and the statistical concentration errors on the horizontal plane near the ground. The velocity errors were small, but the pollutant concentration errors were significant. This meant that the value of turbulence diffusion had a greater influence on the concentration distribution and a smaller influence on the velocity distribution. The performance of each model in the error of concentration was consistent with that in the concentration contour. The dynamic Smagorinsky model performed the best, followed by FFD with no turbulence model, and then the Smagorinsky model. FFD and CFD with RNG k-ε turbulence model had lower accuracy, which was because of the overestimation of turbulent diffusion.

Table 9 Summary of simulation accuracy.

Turbulence model	CFD+RNG k-ε turbulence model	FFD + No turbulence model	FFD+ RNG k-ε turbulence model	FFD + Smagorinsky model	FFD + Dynamic Smagorinsky model
Velocity NRMSE	12.42%	15.53%	12.85%	12.76%	12.03%
Concentration NRMSE	114.51%	80.73%	112.25%	87.43%	69.62%

4.4. Computing time

All the simulations were carried out on a computer with a single Intel CPU at 2.40 GHz. Table 10 listed the computing times for all simulations. The simulation of FFD with different turbulence models was implemented in OpenFOAM, which could count the total computing time and the computing time of different equations by adding user-defined codes. There was only the total computing time that could be obtained in CFD with RNG k-ε turbulence model because it was conducted in ANSYS Fluent 14.0, which could not count the computing time of different parts. The total computing time of CFD was 15.9-61.3 times that of FFD, and the reduction of computing time varied with the used model and simulated case. The total

computing times of FFD without turbulence model, with the Smagorinsky model, and with the dynamic Smagorinsky model were 0.56–0.68, 0.88–0.94 and 1.26–1.34 times that of FFD with RNG k-ε turbulence model, respectively. The speed ratio varied with the simulated case. The computing time without turbulence model was the shortest because it did not need to calculate the eddy viscosity μ_t. The RNG k-ε turbulence model required a considerable amount of time to solve two partial differential equations to obtain μ_t, resulting in long computing time. The time to calculate μ_t of the Smagorinsky and dynamic Smagorinsky models were 0.31–0.38 and 1.65–1.96 times, respectively, that of the RNG k-ε turbulence model. The Smagorinsky model calculated μ_t through an algebraic expression, whereas the dynamic calculation of model coefficient in the algebraic expression of the dynamic Smagorinsky model was time consuming.

Table 10 Summary of the computing time used by FFD and CFD.

Case	Turbulence model	Time for U Eqn (s)	Time for P Eqn (s)	Time for C Eqn (s)	Time for μ_t (s)	Total time (s)
Single building	CFD + RNG k-ε turbulence model	-	-	-	-	124766
	FFD + No turbulence model	713	946	374	3	2036
	FFD + RNG k-ε turbulence model	945	1387	262	731	3325
	FFD + Smagorinsky model	865	1547	343	285	3040
	FFD + Dynamic Smagorinsky model	1148	1664	221	1436	4469
Three buildings	CFD + RNG k-ε turbulence model	-	-	-	-	192833
	FFD + No turbulence model	2118	3471	518	3	6110
	FFD + RNG k-ε turbulence model	2860	3603	528	2053	9044
	FFD + Smagorinsky model	2685	4466	679	649	8478
	FFD + Dynamic Smagorinsky model	3434	4158	608	3893	12094
Array of buildings	CFD + RNG k-ε turbulence model	-	-	-	-	439818
	FFD + No turbulence model	5469	5354	1357	51	12231
	FFD + RNG k-ε turbulence model	6755	8520	1356	5111	21742
	FFD + Smagorinsky model	5841	10295	1379	1613	19129
	FFD + Dynamic Smagorinsky model	7519	10081	1444	8443	27488

5. Discussion

Fast and accurate simulation method could be widely used in outdoor environment, such as the design of industrial plants and residential quarters, etc. The improvement of computing efficiency could greatly reduce the design time and accelerate the progress of the project.

The constant of the Smagorinsky model that we used in this study was a commonly used value of 0.18. Some studies used other values to simulate outdoor environments (Tominaga, & Mochida, 2016). We also performed simulations of Smagorinsky model with different model coefficients and found that the decrease of the coefficient might increase or decrease the accuracy of the velocity and concentration results, but they were lower than the accuracy of the result of dynamic Smagorinsky model. The above results indicated that the coefficient should vary with location to adapt to different flow characteristics. Calculating model coefficient dynamically could provide more accurate predictions.

Dynamic Smagorinsky model was the most accurate model among these several models. However, compared with the experimental results, further improvement was needed to achieve higher efficiency and accuracy.

6. Conclusions

This study evaluated the accuracy and computing efficiency of CFD with the RNG k-ε turbulence model, FFD without turbulence model, with the RNG k-ε turbulence model, with the Smagorinsky model and with the dynamic Smagorinsky model. The evaluation used experimental data on airflow and pollutant dispersion from cases of a single building, three buildings and an array of buildings as the benchmark. The results led to the following conclusions:

(1) Compared with CFD with the RNG k-ε turbulence model, FFD with the RNG k-ε turbulence model can greatly improve the computing speed without reducing the accuracy.

(2) FFD without turbulence model required the least computing time but may cause great errors in some complex cases. When the geometric model of the case was relatively simple or the flow was close to laminar, it also had acceptable accuracy and can be applied.

(3) The difference between the accuracy of FFD with the RNG k-ε turbulence model and Smagorinsky model was not big. But the computing time of FFD with Smagorinsky model was shorter than that of FFD with the RNG k-ε turbulence model. This showed that FFD with Smagorinsky model can increase the computing speed while ensuring accuracy.

(4) Compared with FFD with the other three turbulence models, FFD with the dynamic Smagorinsky model had the most accurate result, and the computing time required will not increase too much. Compared with CFD with RNG k-ε turbulence model, FFD with dynamic Smagorinsky model can improve the accuracy while increasing the computing speed by 16-28 times. It can be widely used in the simulation.

This study found that FFD with Smagorinsky model can increase the computing speed while ensuring the same accuracy as RNG k-ε turbulence model. But their results were not always accurate. The dynamic Smagorinsky model ensured the accuracy of all simulations with much less computing time than CFD with RNG k-ε turbulence model. Therefore, we would recommend the use of FFD with the dynamic Smagorinsky model for outdoor airflow and pollutant dispersion studies.

ACKNOWLEDGEMENT

This study was partially supported by the National Natural Science Foundation of China (NSFC) through grant No. 52108084 and by the China Postdoctoral Science Foundation through Grant No. 2020M680886. We acknowledged financial support from Stiftelsen för

internationalisering av högre utbild-ning och forskning (STINT), Sweden (Dnr: CH2020-8665).

References

ANSYS. (2011). ANSYS Fluent 14.0 Documentation. ANSYS, Inc., canonsburg, PA.

Bahloul, A., Stathopoulos, T., Hajra, B., & Chavez, M. (2014). The effect of upstream and downstream buildings on dispersion of effluents. IRSST research report R-849, Institut de recherche Robert-Sauve´en sante´et en se´curite´du travail, Montreal, Canada.

Blocken, B. (2015). Computational Fluid Dynamics for urban physics: Importance, scales, possibilities, limitations and ten tips and tricks towards accurate and reliable simulations. Building & Environment, 91, 219-245.

Blocken, B., Stathopoulos, T., Carmeliet, J., & Hensen, J. (2009, July). Application of CFD in building performance simulation for the outdoor environment. Eleventh International Building Performance Simulation Association Conference, Glasgow, Scotland.

Chavez, M., Hajra, B., Stathopoulos, T., & Bahloul, A. (2011). Near-field pollutant dispersion in the built environment by CFD and wind tunnel simulations. Journal of Wind Engineering and Industrial Aerodynamics, 99(4), 330-339.

Chavez, M., Stathopoulos, T., & Bahloul, A. (2015, June). CFD simulations for placement of air intakes on buildings and pollutant re-ingestion in the urban environment. The 14th international conference on Wind Engineering, Porto Alegre, Brazil.

Chen, Q., & Xu, W.-R. (1998). A zero-equation turbulence model for indoor airflow simulation, Energy and Buildings, 28, 137-144.

Cole, M., Elliott, R. J. R., & Shimamoto, K. (2005). Industrial characteristics, environmental regulations and air pollution: an analysis of the UK manufacturing sector. Journal of Environmental Economics and Management, 50(1), 121-143.

Ebrahimi, M., & Jahangirian, A. (2013). New analytical formulations for calculation of dispersion parameters of Gaussian model using parallel CFD. Environmental Fluid Mechanics, 13(2), 125-144.

Fedkiw, R., Stam, J., & Jensen, H. W. (2001, August). Visual simulation of smoke. Proceedings of the 28th annual conference on Computer Graphics and Interactive Techniques, Los Angeles, USA.

Franke, J., & Baklanov, A. (2007). Best practice guideline for the CFD simulation of flows in the urban environment: COST action 732 quality assurance and improvement of microscale meteorological models. Brussels, COST Office.

Germano, M., Piomelli, U., Moin, P., & Cabot, W. H. (1990). A dynamic subgrid-scale eddy viscosity model. Physics of Fluids, 3(3), 1760-1765.

Gnedin, N., Semenov, V. Y., & Kravtsov, A. V. (2018). Enforcing the courant–friedrichs–lewy condition in explicitly conservative local time stepping schemes. Journal of Computational Physics, 359, 93-105.

Gousseau, P., Blocken, B., Stathopoulos, T., & van Heijst, G.J.F. (2011). CFD simulation of near-field pollutant dispersion on a high-resolution grid: A case study by LES and RANS for a building group in downtown montreal. Atmospheric Environment, 45(2), 266-279.

Guermond, J. L., Minev, P. D., & Shen, J. (2006). An overview of projection methods for incompressible flows. Computer Methods in Applied Mechanics and Engineering, 195 (44-47), 6011–6045.

He, Y.-H., Liu, X.-H., Zhang, H.-L., & Zheng, W. (2021). Hybrid framework for rapid evaluation of wind environment around buildings through parametric design, CFD simulation, image processing and machine learning, Sustainable Cities and Society, 73, 103092.

Hajra, B., Stathopoulos, T., & Bahloul, A. (2013). A wind tunnel study of the effects of adjacent buildings on near-field pollutant dispersion from rooftop emissions in an urban environment. Journal of Wind Engineering and Industrial Aerodynamics, 119, 133-145.

Hajra, B., Stathopoulos, T., & Bahloul, A. (2010). Assessment of pollutant dispersion from rooftop stacks: ASHRAE, ADMS and wind tunnel simulation. Building & Environment, 45(12), 2768-2777.

Holmes, N., & Morawska, L. (2006). A review of dispersion modelling and its application to the dispersion of particles: An overview of different dispersion models available. Atmospheric Environment, 40(30), 5902-5928.

Jandaghian, Z. (2018). Flow and pollutant dispersion model in a 2D urban street canyons using computational fluid dynamics. Computational Engineering and Physical Modeling, 1(1), 83–93.

Jandaghian, Z., Mortezazadeh, M., & Wang, L. (2018, May). Flow and pollutant dispersion in urban street canyons: Semi-Lagrangian approach with zero equation turbulence model. Tenth International Building

Performance Simulation Association Conference, Montréal, Canada.
Jin, M.-G., Liu, W., & Chen, Q. (2014). Accelerating fast fluid dynamics with a coarse-grid projection scheme, HVAC & R Research, 20(8), 932-943,
Katal, A., Mortezazadeh, M., & Wang, L. (2019). Modeling building resilience against extreme weather by integrated CityFFD and CityBEM simulations, Applied Energy, 250(15), 1402-1417.
[dataset] Leitl, B., & Schatzmann, M. Cedval at Hamburg University, (2010). Compilation of experimental data for validation of microscale dispersion models. https://mi-pub.cen.uni-hamburg.de/ index.php?id=432.
Li, M., Li C., & Zhang, M. (2018). Exploring the spatial spillover effects of industrialization and urbanization factors on pollutants emissions in China's Huang-Huai-Hai region. Journal of Cleaner Production, 195(10), 154-162.
Lin, C., Ooka, R., Kikumoto, H., & Sato, T. (2020). Wind tunnel experiment on high-buoyancy gas dispersion around isolated cubic building. Journal of Wind Engineering and Industrial Aerodynamics, 202, 104-226.
Liu, S.-M., Pan, W.-X., Zhang, H., Cheng, X.-L., & Long, Z.-W. (2017). CFD simulations of wind distribution in an urban community with a full-scale geometrical model. Building & Environment, 117, 11-23.
Liu, W., You, R.-Y., Zhang, J., & Chen, Q. (2017). Development of a fast fluid dynamics-based adjoint method for the inverse design of indoor environments, Journal of Building Performance Simulation, 10(3), 326-343.
Lotrecchiano, N., Sofia, D., Giuliano, A., Barletta, D., & Poletto, M. (2020). Pollution Dispersion from a Fire Using a Gaussian Plume Model. International Journal of Safety and Security Engineering, 10(4), 431-439.
López, A., Nicholls, W., Stickland, M. T., & Dempster, W. M. (2015). CFD study of Jet Impingement Test erosion using Ansys Fluent and OpenFOAM. Computer Physics Communications, 197, 88–95.
Lysenko, D. A., Ertesvåg, I. S., & Rian, K. E. (2013). Modeling of turbulent separated flows using OpenFOAM. Computers & Fluids, 80(1), 408–422.
Mangia, C., Degrazia, G. A., & Rizza, U. (2000). An integral formulation for the dispersion parameters in a shear–buoyancy-driven planetary boundary layer for use in a Gaussian model for tall stacks. Journal of Applied Meteorology, 39(11), 1913-1922.
Mei, S.-J., Luo, Z.-W., Zhao, F.-Y., & Wang, H.-Q. (2019). Street canyon ventilation and airborne pollutant dispersion: 2-D versus 3-D CFD simulations, Sustainable Cities and Society, 50, 101700.
Mortezazadeh, M. (2019). CityFFD – city fast fluid dynamics model for urban microclimate simulations. PhD thesis, Concordia University.
Mortezazadeh, M., & Wang, L. (2018, February). Modelling Urban Airflows by a New Parallel High-Order Semi-Lagrangian 3D Fluid Flow Solver. The 4th International Conference On Building Energy, Environment, Melbourne, Australia.
Mortezazadeh, M., & Wang, L. (2020). Solving city and building microclimates by fast fluid dynamics with large timesteps and coarse meshes. Building & Environment, 179, 106955.
Murakami, S., Iizuka, S., & Ooka, R. (1999). CFD analysis of turbulent flow past square cylinder using dynamic LES. Journal of Fluids and Structures, 13(7-8), 1097-1112.
Overcamp, T. J. (1976). A general Gaussian diffusion-deposition model for elevated point sources. Journal of Applied Meteorology, 15(11), 1167-1171.
Palida, Y., Yu, H.-F., & Wu, W.-Q. (2009). Wind tunnel experiment and numerical simulation on over-head road pollution around a building diffusion and dispersion. Journal of Engineering Thermophysics, 30(9), 1485-1488.
Petersen, R. L., Cochran, B., & Carter, J. J. (2002). Specifying exhaust and intake systems. ASHRAE Journal, 44(8), 30,32-37.
Qin, H.-Q., Hong, B., Huang, B., Cui, X., & Zhang, T. (2020). How dynamic growth of avenue trees affects particulate matter dispersion: CFD simulations in street canyons, Sustainable Cities and Society, 61, 102331.
Smagorinsky, J. (1963). General circulation experiments with the primitive equations. I. The basic experiment, Monthly Weather Review, 91(3), 99-164.
Stam, J. (1999, August). Stable fluids. Proceedings of the 26th annual conference on Computer Graphics and Interactive Techniques, Los Angeles, USA.
Stathopoulos, T., Hajra, B., & Bahloul, A. (2008). Analytical evaluation of dispersion of exhaust from rooftop stacks on buildings. Studies and Research Projects/Report R-576, Montréal.
[dataset] Tanaka, H., Yoshie, R., & Cheng, H.-H. Tokyo Polytechnic University, (2006). Database on Indoor/Outdoor Air Pollution. http://www.wind.arch.t-kougei.ac.jp/info_center/pollution/pollution. html.

Tominaga, Y., & Mochida, Da. (2016). AIJ benchmarks for validation of CFD simulations applied to pedestrian wind environment around buildings. Architectural Institute of Japan.
Tominaga, Y., Mochida, A., Yoshie, R., Kataoka, H., Nozu, T., Yoshikawa, M., & Shirasawa,T. (2008). AIJ guidelines for practical applications of CFD to pedestrian wind environment around buildings. Journal of Wind Engineering and Industrial Aerodynamics, 96(10-11), 1749-1761.
Tominaga, Y., Mochida, A., Murakami, S., & Sawaki, S. (2008). Comparison of various revised k–ε models and LES applied to flow around a high-rise building model with 1:1:2 shape placed within the surface boundary layer. Journal of Wind Engineering and Industrial Aerodynamics, 96(4), 389-411.
Tominaga, Y., & Stathopoulos, T. (2010). Numerical simulation of dispersion around an isolated cubic building: Model evaluation of RANS and LES. Building and Environment, 45(10), 2231-2239.
Tseng, Y.-H., Meneveau, C., & Parlange, M. B. (2006). Modeling flow around bluff bodies and predicting urban dispersion using large eddy simulation. Environmental Science and Technology, 40(8), 2653-2662.
Wang, H.-D., & Zhai, Z. (2012). Application of coarse grid CFD on indoor environment modeling: Optimizing the trade-off between grid resolution and simulation accuracy. HVAC & R research, 18(5), 915-933.
Welahettige, P., & Vaagsaether, K. (2016, September). Comparison of OpenFoam and ANSYS Fluent Computational Fluid Dynamic Simulation of Gas-Gas Single Phase Mixing with and without Static Mixer. The 9th EUROSIM & 57th SIMS Congress on Modelling and Simulation, Oulu, Finland.
Weller, H. G., Tabor, G., Jasak, H., & Fureby, C. (1998). A tensorial approach to computational continuum mechanics using object-oriented techniques. Computers in Physics, 12(6), 620–631.
Wilcox, D. C. (2006). Turbulence Modeling for CFD. 2nd Edition, DCW Industries, Le Canada, California, USA.
Yakhot, V., & Orszag, S. A. (1986). Renormalization group analysis of turbulence. I. Basic Theory. Journal of Scientific Computing, 1(1), 3–51.
Yu, H.-S., & The, J. (2017). Simulation of Gaseous Pollutant Dispersion Around an Isolated Building using the k-ω SST Turbulence Model. Journal of the Air & Waste Management Association, 67(5), 517-536.
Zhang, S.-W., Kwok, K. C. S., Liu, H.-H., Jiang, Y.-C., Dong, K.-J., & Wang, B. (2021). A CFD study of wind assessment in urban topology with complex wind flow, Sustainable Cities and Society, 71, 103006.
Zuo,W., & Chen, Q. (2009). Real time or faster-than-real-time simulation of airflow in buildings. Indoor Air, 19(1), 33-44.
Zuo, W., & Chen, Q. (2010). Simulations of air distributions in buildings by FFD on GPU. HVAC & R Research, 16(6), 785–798.
Zuo, W., Hu, J.-J., & Chen, Q. (2010). Improvements on FFD modeling by using different numerical schemes. Numerical Heat Transfer, Part B: Fundamentals, 58(1), 1-16.

Appendix A

In the single-building case, we tested grids with 0.109 million, 0.372 million and 1.263 million cells, as shown in Fig.A.1. The stretching ratios of the three grids were 1.090, 1.075 and 1.055, respectively, which met the requirement of less than 1.3. The evaluation height was located at the third, fourth and sixth grid above the ground, respectively, which met the requirement of not lower than the third grid. The refinement ratios for two consecutive grids were 3.41 and 3.39, which met the requirement of greater than 3.375. The grid number of 0.372 million was found that provided grid-independent results, as shown in Fig.A.2.

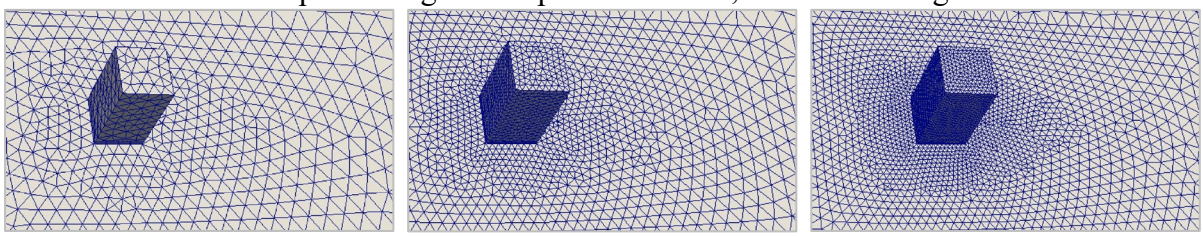

(a) (b) (c)

Fig. A.1. The meshes of (a) 0.109 million, (b) 0.372 million and (c) 1.263 million grid numbers for a single building case

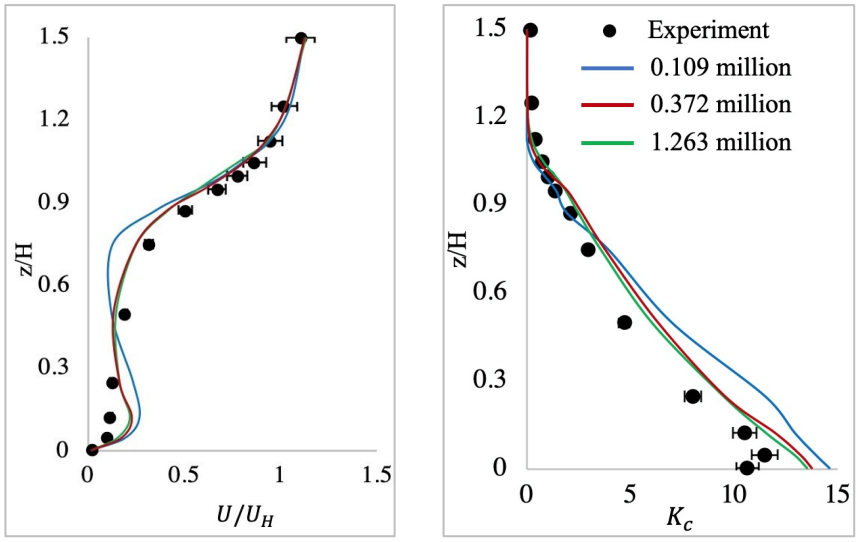

(a) (b)

Fig. A.2. Comparison of (a) the normalized scalar velocity and (b) the normalized concentration between results of the three mesh systems and the measured values at x = 0.75H on the center vertical plane

In the three-building case, we tested grids with 0.285 million, 0.973 million and 3.293 million cells, as shown in Fig.A.3. The stretching ratios of the three grids were 1.070, 1.065 and 1.060, respectively, which met the requirement of less than 1.3. The evaluation height was located at the third, fourth and sixth grid above the ground, respectively, which met the requirement of not lower than the third grid. The refinement ratios for two consecutive grids were 3.41 and 3.38, which met the requirement of greater than 3.375. The grid number of 0.973 million was found that provided grid-independent results, as shown in Fig.A.4.

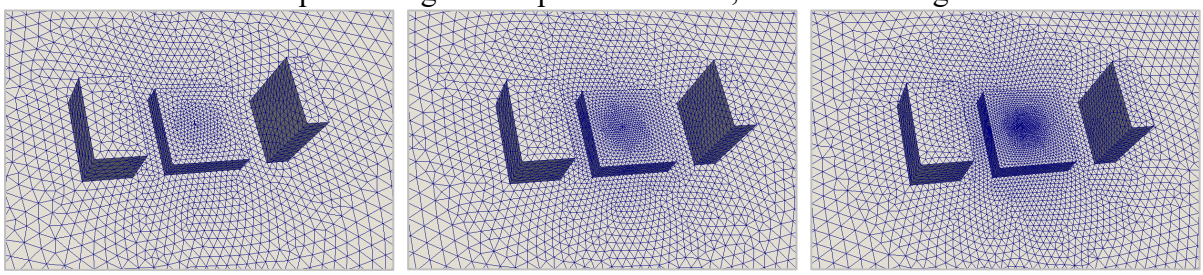

(a) (b) (c)

Fig. A.3. The meshes of (a) 0.285 million, (b) 0.973 million and (c) 3.293 million grid numbers for a three-building case

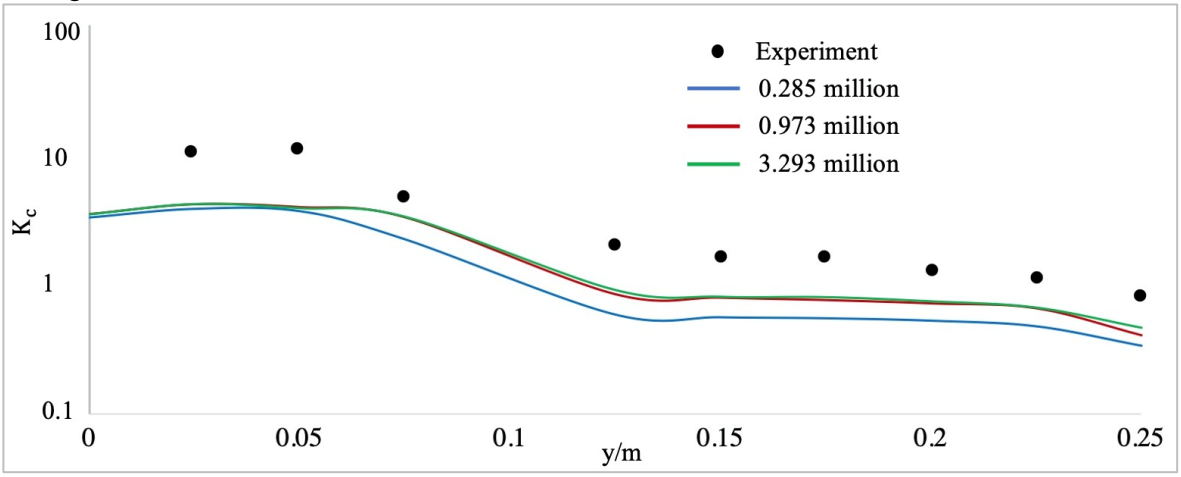

Fig. A.4. Comparison of the normalized concentration between results of the three mesh systems and the measured values on the central horizontal line on the roof

In the array of buildings case, we tested grids with 0.438 million, 1.503 million and 5.159 million cells, as shown in Fig.A.5. The stretching ratios of the three grids were 1.055, 1.060 and 1.055, respectively, which met the requirement of less than 1.3. The evaluation height was located at the third, fifth and seventh grid above the ground, respectively, which met the requirement of not lower than the third grid. The refinement ratios for two consecutive grids were 3.42 and 3.43, which met the requirement of greater than 3.375. The grid number of 1.503 million was found that provided grid-independent results, as shown in Fig.A.6.

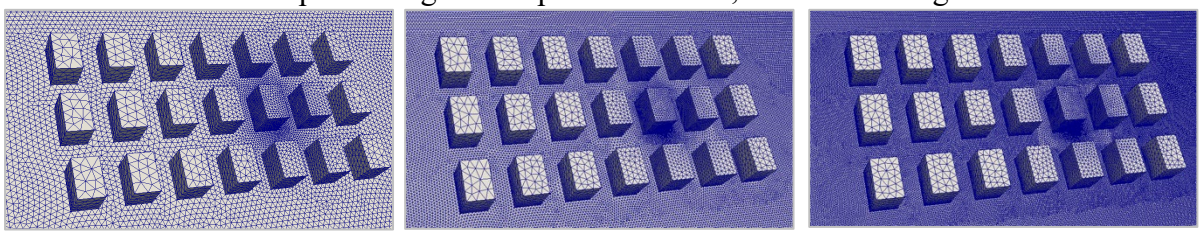

Fig. A.5. The meshes of (a) 0.438 million, (b) 1.503 million and (c) 5.159 million grid numbers for the array of buildings case

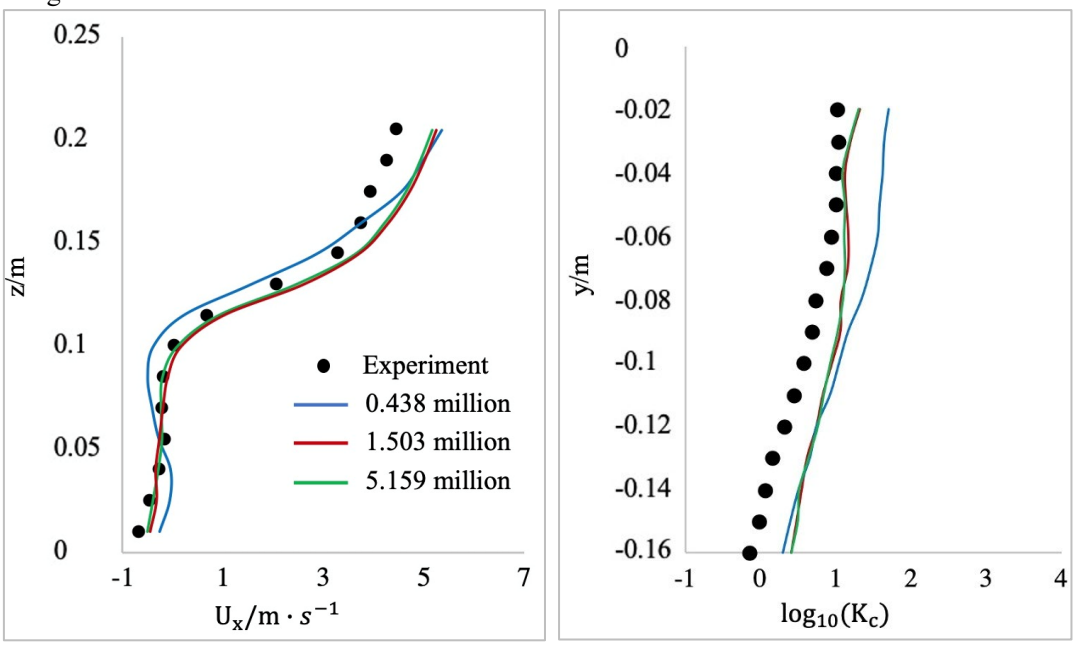

(a) (b)

Fig. A.6. Comparison of the (a) normalized velocity in the *z*-direction on a vertical line and (b) normalized concentration in the *y*-direction on a horizontal line between the simulation result of three mesh systems and the corresponding experimental data